Inorg. Chem. **2007**, *46*, 9863–9872

Electron-Transfer-Catalyzed Rearrangement of Unsymmetrically Substituted Diiron Dithiolate Complexes Related to the Active Site of the [FeFe]-Hydrogenases

Salah Ezzaher, Jean-François Capon, Frédéric Gloaguen, François Y. Pétillon, Philippe Schollhammer,* and Jean Talarmin*

UMR CNRS 6521, Chimie, Electrochimie Moléculaires et Chimie Analytique, UFR Sciences et Techniques, Université de Bretagne Occidentale, CS 93837, 29238 Brest-Cedex 3, France

Received July 4, 2007

Novel asymmetrically substituted azadithiolate compounds $[Fe_2(CO)_4(\kappa^2\text{-dppe})\{\mu\text{-}SCH_2N(R)CH_2S\}]$ (R = ^{i}Pr, **1a**; $CH_2CH_2OCH_3$, **1b**; $CH_2C_6H_5$, **1c**) have been synthesized by treatment of $[Fe_2(CO)_6(\mu\text{-adt})]$ [adt = $SCH_2N(R)CH_2S$, with R = ^{i}Pr, $CH_2CH_2OCH_3$, $CH_2C_6H_5$] with dppe (dppe = $Ph_2PCH_2CH_2PPh_2$) in refluxing toluene in the presence of Me_3NO. **1a**–**c** have been characterized by single-crystal X-ray diffraction analyses. The electrochemical investigation of **1a**–**c** and of $[Fe_2(CO)_4(\kappa^2\text{-dppe})(\mu\text{-pdt})]$ (**1d**) [pdt = $S(CH_2)_3S$] in MeCN– and THF–$[NBu_4][PF_6]$ has demonstrated that the electrochemical reduction of **1a**–**d** gives rise to an Electron-transfer-catalyzed (ETC) isomerization to the symmetrical isomers **2a**–**d** where the dppe ligand bridges the iron centers. Compounds **2a**–**d** were characterized by IR and NMR spectroscopy, elemental analysis, and X-ray crystallography for **2a**.

Introduction

The discovery[1] that the [FeFe]-hydrogenases use an organometallic diiron dithiolate center with CO and CN^- ligands to efficiently catalyze the H^+/H_2 conversion is at the origin of the revival of the chemistry of $[Fe_2(CO)_{6-n}(L)_n(\mu\text{-dithiolate})]$ complexes.[2] A variety of models of the [2Fe] subsite of the H-cluster are now known,[2,3] and recent efforts have been directed toward the synthesis of unsymmetrically substituted diiron dithiolate complexes, with well differentiated metal centers, that would mimic more closely the biological site.[4−9] Quite remarkably, an artificial H-cluster model of the biological site has been synthesized.[10]

A new generation of diiron complexes with polydentate ligands has emerged very recently, which should permit one to examine the effect of introducing an asymmetrical feature

* To whom correspondence should be addressed. E-mail: jean.talarmin@univ-brest.fr (J.T.); schollha@univ-brest.fr (P.S.).

(1) (a) Peters, J. W.; Lanzilotta, W. N.; Lemon, B. J.; Seefeldt, L. C. *Science* **1998**, *282*, 1853−1858. (b) Nicolet, Y.; Piras, C.; Legrand, P.; Hatchikian, C. E.; Fontecilla-Camps, J. C. *Structure* **1999**, *7*, 13−23. (c) Nicolet, Y.; de Lacey, A. L.; Vernede, X.; Fernandez, V. M.; Hatchikian, C. E.; Fontecilla-Camps, J. C. *J. Am. Chem. Soc.* **2001**, *123*, 1596−1602. (d) Lemon, B. J.; Peters, J. W. *Biochemistry* **1999**, *38*, 12969−12973.

(2) For recent reviews, see: (a) Georgakaki, I. P.; Thomson, L. M.; Lyon, E. J.; Hall, M. B.; Darensbourg, M. Y. *Coord. Chem. Rev.* **2003**, *238*−*239*, 255−266. (b) Darensbourg, M. Y.; Lyon, E. J.; Zhao, X.; Georgakaki, I. P. *Proc. Natl Acad. Sci. U.S.A.* **2003**, *100*, 3683−3688. (c) Evans, D. J.; Pickett, C. J. *Chem. Soc. Rev.* **2003**, *32*, 268−275. (d) Rauchfuss, T. B. *Inorg. Chem.* **2004**, *43*, 14−26. (e) Song, L.-C. *Acc. Chem. Res.* **2005**, *38*, 21−28. (f) Artero, V.; Fontecave, M. *Coord. Chem. Rev.* **2005**, *249*, 1518−1535. (g) Best, S. P. *Coord. Chem. Rev.* **2005**, *249*, 1536−1554. (h) Bruschi, M.; Zampella, G.; Fantucci, P.; De Gioia, L. *Coord. Chem. Rev.* **2005**, *249*, 1620−1640. (i) Liu, X.; Ibrahim, S. K.; Tard, C.; Pickett, C. J. *Coord. Chem. Rev.* **2005**, *249*, 1641−1652. (j) Sun, L.; Åkermark, B.; Ott, S. *Coord. Chem. Rev.* **2005**, *249*, 1653−1663. (k) Capon, J.-F.; Gloaguen, F.; Schollhammer, P.; Talarmin, J. *Coord. Chem. Rev.* **2005**, *249*, 1664−1676. (l) Vignais, P. *Coord. Chem. Rev.* **2005**, *249*, 1677−1690, and references cited therein.

(3) For {2Fe3S} complexes, see: (a) Razavet, M.; Davies, S. C.; Hughes, D. L.; Barclay, J. E.; Evans, D. J.; Fairhurst, S. A.; Liu, X.; Pickett, C. J. *Dalton Trans.* **2003**, 586−595. (b) George, S. J.; Cui, Z.; Razavet, M.; Pickett, C. J. *Chem. Eur. J.* **2002**, *8*, 4037−4046. (c) Zampella, G.; Bruschi, M.; Fantucci, P.; Razavet, M.; Pickett, C. J.; de Gioia, L. *Chem. Eur. J.* **2005**, *11*, 509−520. (d) Lawrence, J. D.; Li, H.; Rauchfuss, T. B. *Chem. Commun.* **2001**, 1482−1483. (e) Song, L.-C.; Yang, Z.-Y.; Bian, H.-Z.; Hu, Q.-M. *Organometallics*, **2004**, *23*, 3082−3084. (f) Hu, M.-Q.; Ma, C.-B.; Zhang, X.-F.; Chen, F.; Chen, C.-N.; Liu, Q.-T. *Chem. Lett.* **2006**, *35*, 840−841. (g) Windhager, J.; Rudolph, M.; Bräutigam, S.; Görls, H.; Weigand, W. *Eur. J. Inorg. Chem.* **2007**, 2748−2760.

(4) Tye, J. W.; Darensbourg, M. Y.; Hall, M. B. *Inorg. Chem.* **2006**, *45*, 1552−1559.

(5) Justice, A. K.; Zampella, G.; de Gioia, L.; Rauchfuss, T. B.; van der Vlugt, J. I.; Wilson, S. R. *Inorg. Chem.* **2007**, *46*, 1655−1664.

(6) (a) Hogarth, G.; Richards, I. *Inorg. Chem. Commun.* **2007**, *10*, 66−70. (b) Adam, F. L.; Hogarth, G.; Richards, I.; Sanchez, B. E. *Dalton Trans.* **2007**, 2495−2498. (c) Adam, F. L.; Hogarth, G.; Richards, I. *J. Organomet. Chem.* **2007**, *692*, 3957−3968.

(7) Duan, L.; Wang, M.; Li, P.; Na, Y.; Wang, M.; Sun, L. *Dalton Trans.* **2007**, 1277−1283.

10.1021/ic701327w CCC: $37.00
Published on Web 10/17/2007

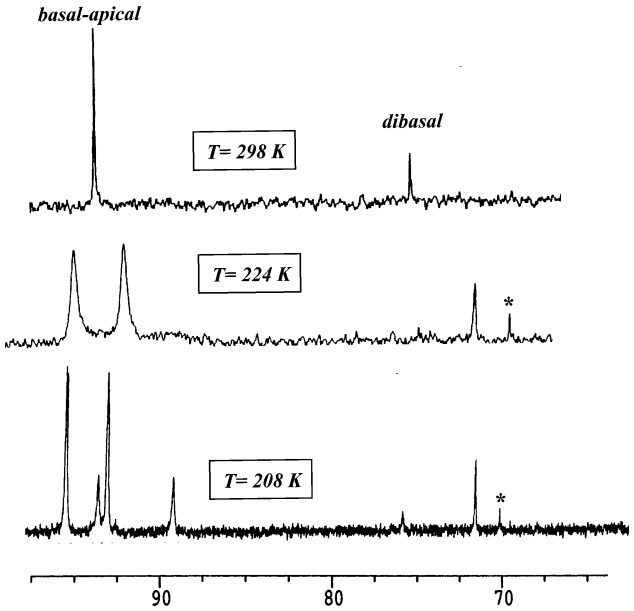

Figure 1. Variable-temperature $^{31}P\{^{1}H\}$ NMR spectra (in CD_2Cl_2) of $[Fe_2(CO)_4(\kappa^2\text{-dppe})\{\mu\text{-}SCH_2N(R)CH_2S\}]$ (R = CH_2CH_2OMe, **1b**) (* = impurity).

Scheme 1

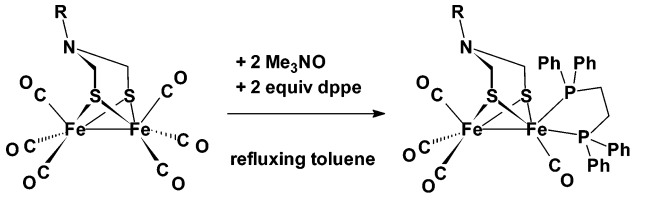

in diiron systems through chelating ligands with the prospect of designing more efficient electrocatalysts.[4−9] A detailed understanding of both the reduction processes and the elementary protonation steps of dithiolate-bridged species is primordial to shedding light on the hydrogenase process. To this end, we have reported the synthesis and the protonation of $[Fe_2(CO)_4(\kappa^2\text{-L})(\mu\text{-pdt})]$ (pdt = $S(CH_2)_3S$) where L is either a chelating bis-(N-heterocyclic carbene) or dppe ligand[8,9] (dppe = $Ph_2P(CH_2)_2PPh_2$). We have now undertaken investigating electrochemically this type of asymmetrically diphos-substituted compounds where an azadithiolate (adt) or a propanedithiolate (pdt) bridges the tetracarbonyl diiron core to assess whether the uneven substitution at the iron centers induces a specific electron-transfer chemistry. Herein, we report the synthesis and the characterization of the novel asymmetrically substituted azadithiolate diiron complexes $[Fe_2(CO)_4(\kappa^2\text{-dppe})\{\mu\text{-}SCH_2N(R)CH_2S\}]$ (R = ^{i}Pr, **1a**; $CH_2CH_2OCH_3$, **1b**; $CH_2C_6H_5$, **1c**),

(8) Morvan, D.; Capon, J.-F.; Gloaguen, F.; Le Goff, A.; Marchivie, M.; Michaud, F.; Schollhammer, P.; Talarmin, J.; Yaouanc, J.-J.; Pichon, R.; Kervarec, N. *Organometallics* **2007**, *26*, 2042−2052.
(9) Ezzaher, S.; Capon, J.-F.; Gloaguen, F.; Pétillon, F.Y.; Schollhammer, P.; Talarmin, J.; Pichon, R.; Kervarec, N. *Inorg. Chem.* **2007**, *46*, 3426−3428.
(10) Tard, C.; Liu, X.; Ibrahim, S. K.; Bruschi, M.; de Gioia, L.; Davies, S. C.; Yang, X.; Wang, L.-S.; Sawers, G.; Pickett, C. J. *Nature* **2005**, *433*, 610−613.

Scheme 2. Enantiomeric Forms of the Basal−Apical Form of Complexes **1**

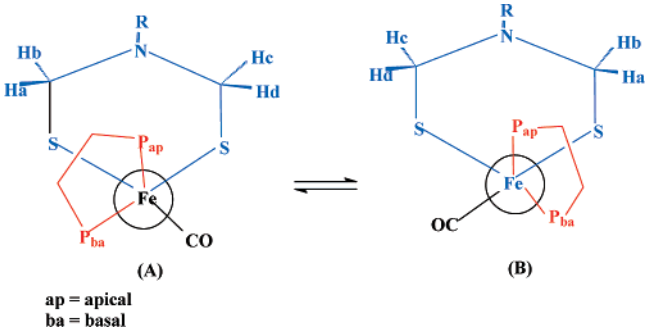

Table 1. Selected Bond Lengths (Å) and Angles (deg) for **1a**−**c**

	1a	1b*	1c#
Fe1−Fe2	2.5451(8)	2.5453(12)	2.5445(11)
Fe1−S1	2.2523(11)	2.2543(16)	2.2471(16)
Fe1−S2	2.2551(11)	2.2571(18)	2.2618(14)
Fe2−S1	2.2621(11)	2.2527(17)	2.2660(15)
Fe2−S2	2.2783(12)	2.2646(17)	2.2793(16)
Fe1−P1	2.2314(11)	2.2318(17)	2.2119(15)
Fe1−P2	2.1987(12)	2.1930(17)	2.1831(16)
N1−C5	1.452(5)	1.435(7)	1.457(6)
N1−C7 (6)*	1.443(5)	1.438(7)	1.456(6)
N1−C50 (34)#	1.493(4)	1.492(8)	1.482(6)
C5−N1−C7(6)*	111.7(3)	112.2(6)	111.9(4)
(6)*C7−N1−C50 (34)#	113.9(3)	112.8(6)	111.7(4)
C5−N1−C50 (34) #	110.9(3)	110.1(5)	107.9(4)
Fe1−S1−Fe2	68.63(3)	68.77(5)	68.64(5)
Fe1−S2−Fe2	68.31(3)	68.51(5)	68.16(4)
P1−Fe1−P2	87.84(4)	87.74(6)	86.95(6)

and we show that the electrochemical reduction of $[Fe_2(CO)_4(\kappa^2\text{-dppe})(\mu\text{-dithiolate})]$ complexes [dithiolate = pdt or adt; $SCH_2N(R)CH_2S$, R = ^{i}Pr, CH_2CH_2OMe, $CH_2C_6H_5$] gives rise to an electron-transfer-catalyzed (ETC)[11] rearrangement to the symmetrical isomer, $[Fe_2(CO)_4(\mu\text{-dithiolate})(\mu\text{-dppe})]$ (**2**).

Results and Discussion

Synthesis and Characterization of $[Fe_2(CO)_4(\kappa^2\text{-dppe})\{\mu\text{-}SCH_2N(R)CH_2S\}]$ (R = ^{i}Pr, 1a; CH_2CH_2OMe, 1b; $CH_2C_6H_5$, 1c). Treatment of $[Fe_2(CO)_6(\mu\text{-adt})]$ with dppe in refluxing toluene for 4 h in the presence of Me_3NO afforded moderate yields of the asymmetric substituted complexes $[Fe_2(CO)_4(dppe)(\mu\text{-adt})]$ (**1**) (Scheme 1).

Compounds **1a**−**c** were characterized by elemental analysis and IR and NMR spectroscopy. Strong ν(CO) bands are observed between 2020 and 1900 cm^{-1} in the infrared spectrum of CH_2Cl_2 solutions of **1a**−**c**. The $^{31}P\{^{1}H\}$ NMR spectra of **1a**−**c** in CD_2Cl_2 show two singlets between 92 and 76 ppm with a ratio of ca. 8:2. Upon cooling, the more deshielded signal splits into two ill-resolved AB quartets and the signal at ca. 76 ppm splits into two singlets (Figure 1). These observations are in accord with previous studies which indicate the presence of four isomers at low temperature for analogous compounds.[5,9] On this basis, the former peak was assigned to a basal−apical isomer and the latter to a basal−basal form, with two possible orientations of the adt bridge for each isomer. Interestingly, the nature of the R group borne by the azadithiolate bridge induces different ratios of the two forms generated by the motion of the adt bridge. Indeed, for

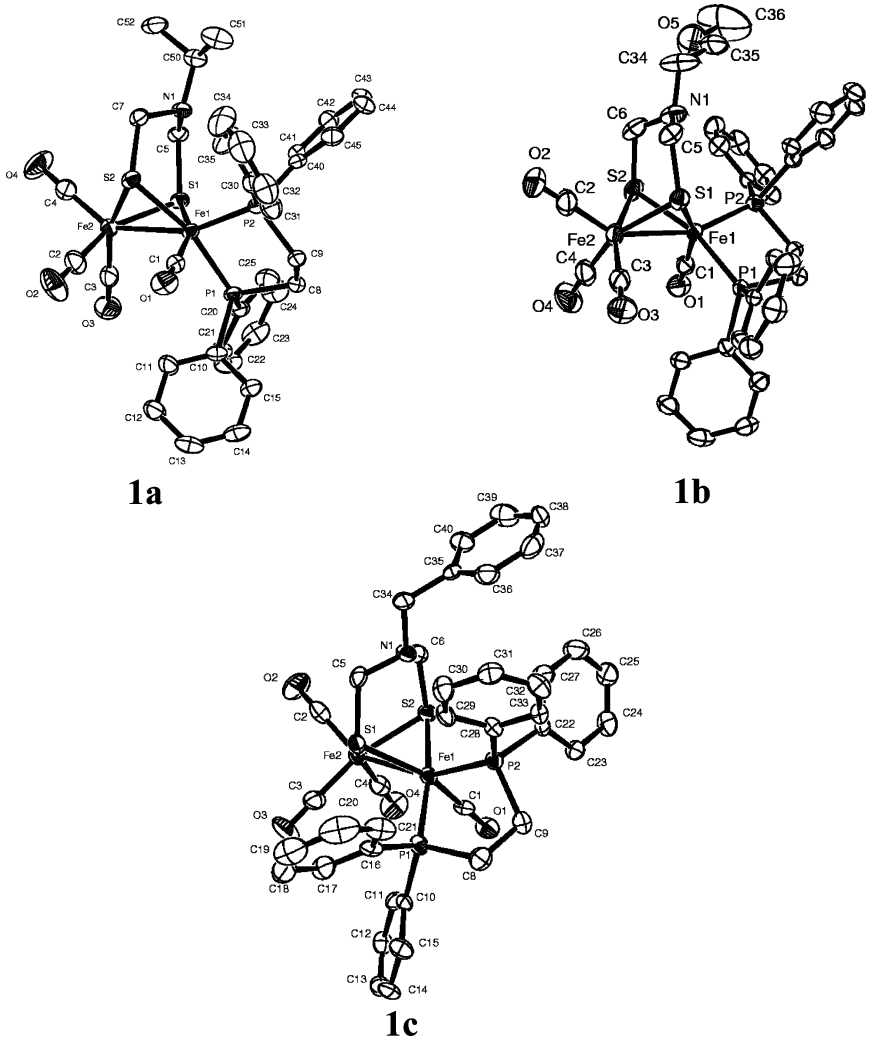

Figure 2. Molecular structures of compounds $[Fe_2(CO)_4(\kappa^2\text{-dppe})\{\mu\text{-}SCH_2N(R)CH_2S\}]$ (R = ^{i}Pr, **1a**; CH_2CH_2OMe, **1b**; $CH_2C_6H_5$, **1c**) with thermal ellipsoids at 30% probability.

both basal−apical and dibasal isomers, 90:10, 70:30, and 60:40 ratios were obtained at 183 K for R = ^{i}Pr, CH_2CH_2-OCH_3, and $CH_2C_6H_5$, respectively. ^{1}H NMR spectra of **1a**−**c** display the set of resonances expected for the various R groups. They confirm the presence of two isomers at 298 K, but full assignment of their resonances could only be proposed for **1a** (R = ^{i}Pr). As expected, temperature dependence of the line shapes was observed for all the complexes by cooling their solutions. For example, at 183 K the ^{1}H NMR spectrum of the major basal−apical form of **1a** displays four doublets at 2.83 (1H), 2.40 (1H), 1.55 (1H), and 1.60 (1H) ppm for the protons of the adt bridge, instead of two doublets at 2.74 (2H) and 1.75 (2H) ppm at room temperature. This confirms that the exchange between the two enantiomers (forms **A** and **B**) and the adt motion are slowed down at low temperature (Scheme 2).

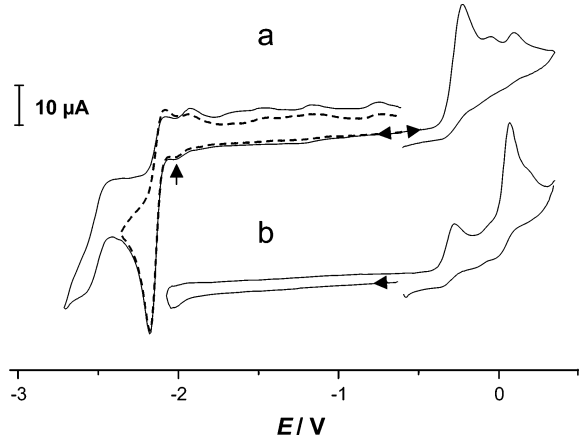

Figure 3. Cyclic voltammetry of $[Fe_2(CO)_4(\kappa^2\text{-dppe})\{\mu\text{-}SCH_2N(^iPr)\text{-}CH_2S\}]$ (**1a**) (1.1 mM). (a) MeCN−$[NBu_4][PF_6]$ under Ar; (b) the potential was held for 10 s at −2.05 V before scan reversal (υ = 0.2 V s^{-1}, vitreous carbon electrode).

X-ray analysis of single crystals of complexes **1a**−**c** obtained from diethyl ether solutions established without any

(11) For reviews on electron-transfer-catalyzed (ETC) processes, see: (a) Chanon, M.; Tobe, M. L. *Angew. Chem., Int. Ed.* **1982**, *21*, 1−23. (b) Chanon, M. *Acc. Chem. Res.* **1987**, *20*, 214−221. (c) Astruc, D. *Angew. Chem., Int. Ed.* **1988**, *27*, 643−660. (d) Astruc, D. *Chem. Rev.* **1988**, *88*, 1189−1216. (e) Kochi, J. K. *J. Organomet. Chem.* **1986**, *300*, 139−166. (f) Hershberger, J. W.; Amatore, C.; Kochi, J. K. *J. Organomet. Chem.* **1983**, *250*, 345−371. (g) Savéant, J. M. *Acc. Chem. Res.* **1980**, *13*, 323−329. (h) Amatore, C.; Pinson, J.; Savéant, J. M.; Thiébault, A. *J. Am. Chem. Soc.* **1982**, *104*, 817−826. (i) Feldberg, S. W.; Jeftic, L. *J. Phys. Chem.* **1972**, *76*, 2439−2446 and references cited therein.

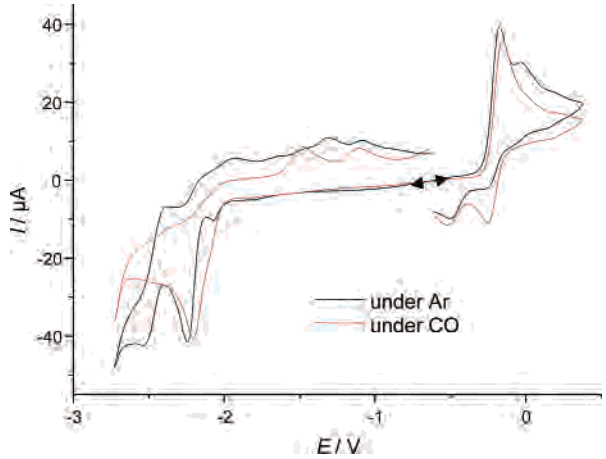

Figure 4. Cyclic voltammetry of $[Fe_2(CO)_4(\kappa^2\text{-dppe})(\mu\text{-pdt})]$ (**1d**) in MeCN−$[NBu_4][PF_6]$ under Ar and under CO (υ = 0.2 V s^{-1}, vitreous carbon electrode).

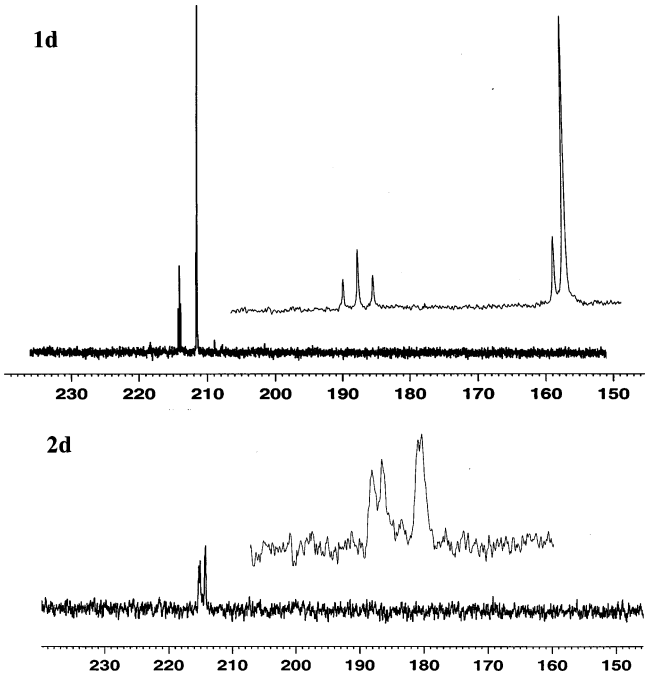

Figure 5. $^{13}C[^1H]$ NMR spectrum of $[Fe_2(CO)_4(\kappa^2\text{-dppe})(\mu\text{-pdt})]$ (**1d**) and $[Fe_2(CO)_4(\mu\text{-pdt})(\mu\text{-dppe})]$ (**2d**) in the CO region at 298 K.

ambiguity their geometry and the binding mode of the bidendate diphosphine to a single iron atom in a basal−apical position (Figure 2 and Table 1). The Fe−P_{ba} (basal position) bond is slightly shorter than the Fe−P_{ap} (apical position) one [Fe1−P_{ba} = 2.2314(11), 2.2318(17), 2.2119(15) Å and Fe1−P_{ap} = 2.1987(12), 2.1930(17), 2.1831(16) Å in **1a**, **1b**, **1c**, respectively]. Other distances and angles are unexceptional. **1** is structurally analogous to other diiron(I) hexacarbonyl adt-bridged complexes.[12] The two {$Fe(CO)_3$} and {Fe(CO)-P_2} units are eclipsed and linked by a direct Fe−Fe bond and the adt group. The resulting coordination geometry around each Fe atom is described as a distorted square pyramid supplemented by the Fe(I)−Fe(I) single bond required by normal electron counting rules. The NR groups lie in an equatorial position and the sum of the C−N−C angles around N1 is between 336° (**1a**) and 330° (**1c**).

Electron Transfer-Catalyzed Rearrangement of $[Fe_2(CO)_4(\kappa^2\text{-dppe})(\mu\text{-}SCH_2XCH_2S)]$ (1) (X = N^iPr, 1a; NCH_2CH_2OMe, 1b; CH_2, 1d). The cyclic voltammetry (CV) of **1a,b,d** in THF- and MeCN-$[NBu_4][PF_6]$ electrolyte revealed that the electrochemical reduction of the complexes gives rise to an ETC[11] process. Indeed, whereas the CV in the oxidation range shows the quasi-reversible or irreversible oxidation of **1a**,**b**,**d** (Table 2, Figures 3a and S1, Supporting Information), the major peaks in the negative domain do not arise from **1** but from a product generated by its reduction. The actual reduction of **1** is characterized by the small peak around −2 V (see arrows in Figures 3a and S1). Experimental evidence for the occurrence of an ETC process upon electrochemical reduction of **1** is as follows.

(1) The current ratio of the minor reduction peak (i_p^{red1})[13] to the major peak at ca. −2.2 V (i_p^{red2}) measured from a MeCN−$[NBu_4][PF_6]$ solution of **1a**,**b**,**d** increases with increasing scan rates (0.04 V $s^{-1} \le \upsilon \le$ 10 V s^{-1}) as expected for an ETC process.

(2) Lowering of the temperature results in an increase of the minor reduction peak at the expense of the peaks situated at more negative potentials.

(3) The product detected by a new oxidation on the reverse scan is generated at the potential of the minor reduction peak, as illustrated in Figure 3b for complex **1a** (and for **1d** in Figure S1b, Supporting Information).

(4) Exhaustive electrolysis of a solution of **1** at the potential of the minor peak produces the symmetrical complex **2** (see below) with a small charge consumption (≤0.5 F mol^{-1} **1**).

The ETC process results from the fast isomerization of $\mathbf{1}^-$ to $\mathbf{2}^-$ that oxidizes at a potential more negative than the reduction of **1**. Therefore, $\mathbf{2}^-$ is oxidized either at the electrode surface (at the reduction potential of **1**) or by **1** in a homogeneous cross-redox reaction (Scheme 3). As a consequence of the oxidation of $\mathbf{2}^-$, the reduction peak of **1** is suppressed and **2** is generated by electrolysis of **1** with a low charge consumed.

The CVs in Figure 4 (also see Figure S2, Supporting Information) are informative as to the mechanism of the rearrangement since the fact that the reduction peak of **1** is larger in the presence of CO (note that the onset of the reduction of **1** under CO is coincident with that under Ar) demonstrates that the catalytic process is less efficient under these conditions. This may arise from the reaction of $\mathbf{1}^-$, $\mathbf{2}^-$, or an intermediate between these species with CO. ETC processes are most frequently associated with substitution reactions that involve notably diiron dithiolate carbonyl

(12) Vijaikanth, V; Capon, J.-F.; Gloaguen, F.; Pétillon, F.Y.; Schollhammer, P.; Talarmin, J. *J. Organomet. Chem.* **2007**, *692*, 4177−4181 and references cited therein.

(13) The parameters i_p and E_p are, respectively, the peak current and the peak potential of a redox process; $E_{1/2} = (E_p^a + E_p^c)/2$; E_p^a, i_p^a and E_p^c, i_p^c are, respectively, the potential and the current of the anodic and of the cathodic peak of a reversible process; $\Delta E_p = E_p^a - E_p^c$. CV stands for cyclic voltammetry; υ (V s^{-1}) is the scan rate in CV experiments. An EC process comprises one electron transfer step (E) followed by a chemical reaction (C).

Table 2. Redox Potentials of $[Fe_2(CO)_4(dppe)\{\mu\text{-dithiolate}\}]$ Complexes as Measured by Cyclic Voltammetry ($\upsilon = 0.2$ V s^{-1} unless Stated Otherwise; Vitreous Carbon Electrode)

complex	solvent	E_p^{red} (V)	E_p^{ox} (V)	detection potentials of products (V)
$[Fe_2(CO)_4(\kappa^2\text{-dppe})\{\mu\text{-}SCH_2N(R)CH_2S\}]$ **1a** (R = ^{i}Pr)	MeCN	−2.01	−0.30	−2.12 ($E_{1/2}$) −2.59 (E_p) 0.07 (E_p^{ox})
	THF	−2.22	−0.21($E_{1/2}$)	−2.32 ($E_{1/2}$) −2.75 ($E_{1/2}$) 0.10 (E_p^{ox})
$[Fe_2(CO)_4(\mu\text{-dppe})\{\mu\text{-}SCH_2N(R)CH_2S\}]$ **2a** (R = ^{i}Pr)	MeCN	−2.12 ($E_{1/2}$)	0.08	−2.59 (E_p) −2.50 ($E_{1/2}$)[a]
$[Fe_2(CO)_4(\kappa^2\text{-dppe})\{\mu\text{-}SCH_2N(R)CH_2S\}]$ **1b** (R = CH_2CH_2OMe)	MeCN	−1.98	−0.26	−2.11 ($E_{1/2}$) −2.49 ($E_{1/2}$) 0.08 (E_p^{ox})
	THF	−2.16	−0.25($E_{1/2}$)	−2.36 (E_p) −2.78 ($E_{1/2}$) 0.13 (E_p^{ox})
$[Fe_2(CO)_4\{\mu\text{-}SCH_2N(R)CH_2S\}(\mu\text{-dppe})]$ **2b** (R = CH_2CH_2OMe)	MeCN	−2.10 ($E_{1/2}$)	0.08	−2.48 ($E_{1/2}$)
	THF	−2.36 ($E_{1/2}$)	0.14 (−0.07)[b]	−2.79 ($E_{1/2}$)
$[Fe_2(CO)_4(\kappa^2\text{-dppe})(\mu\text{-pdt})]$ **1d**	MeCN	−2.07	−0.20	−2.22 (E_p) −2.43 ($E_{1/2}$) 0.18 (E_p^{ox})
	THF	−2.12	−0.07	−2.37 (E_p) −2.60 ($E_{1/2}$) 0.43 (E_p^{ox})
$[Fe_2(CO)_4(\mu\text{-pdt})(\mu\text{-dppe})]$ **2d**	MeCN	−2.23 −2.12 ($E_{1/2}$)[c]	0.17 (−0.04)[b]	−2.43 ($E_{1/2}$)
	THF	−2.37 −2.32 ($E_{1/2}$)[d]	0.41 (0.15)[b]	−2.59 ($E_{1/2}$)

[a] $\upsilon = 2$ V s^{-1}. [b] Reduction peak (E_p^{red}) on the return scan. [c] $\upsilon = 5$ V s^{-1}. [d] $\upsilon = 1$ V s^{-1}.

Scheme 3

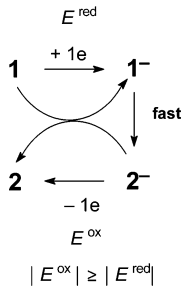

Scheme 4

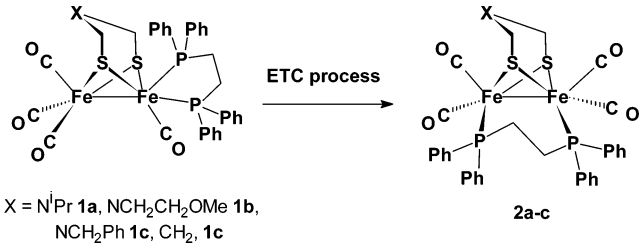

complexes,[14] while examples of ETC isomerization are still rare[15] and are unprecedented for dithiolate-bridged diiron complexes. An analysis of the mechanism of the catalytic process will be presented below.

Electron-Transfer Catalyzed Synthesis and Characterization of $[Fe_2(CO)_4(\mu\text{-}SCH_2XCH_2S)(\mu\text{-dppe})]$ (2) (X = N^{i}Pr, 2a; NCH$_2$CH$_2$OMe, 2b; NCH$_2$C$_6$H$_5$, 2c; CH$_2$, 2d). Controlled-potential electrolyses of brown solutions of **1a**−**d** carried out at the potential of the minor reduction peak were complete after the passage of 0.1−0.5 F mol^{-1} **1a**−**d**. The CV of the bright red catholyte showed that **2a**−**d** formed essentially quantitatively (Scheme 4, Figure S3, Supporting Information). Electrolyses performed in THF−$[NBu_4][PF_6]$ on a preparative scale (0.1−0.2 g of **1**) consumed comparatively less charge (0.08−0.15 F mol^{-1}) than when smaller amounts of complex are used, suggesting that homogeneous redox steps contribute significantly to the formation of the product. Complexes **2a**−**d** were extracted from the catholyte and fully characterized by NMR spectroscopy, elemental analysis, and X-ray crystallography for **2a** (see below and Experimental Section). ^{1}H NMR spectra of these compounds show the presence of only one isomer in solution with the expected signals for the R groups. ^{31}P NMR spectra of complexes **2** display one signal at ca. 60 ppm that accords with those observed for analogous derivatives.[6c,16] The comparison of their ^{13}C NMR spectra at 298 K with those of their precursors indicates a characteristic change of the carbonyl pattern (see Figure 5). A singlet and a triplet (J = 20 Hz) are dectected at 212.7 and 215.3 ppm, respectively, for the asymmetrically substituted complex $[Fe_2(CO)_4(\kappa^2\text{-dppe})(\mu\text{-pdt})]$. These signals are assigned unambigously to

(14) (a) Darchen, A.; Mousser, H.; Patin, H. *J. Chem. Soc., Chem. Commun.* **1988**, 968−970. (b) Gloaguen, F.; Morvan, D.; Capon, J.-F.; Schollhammer, P.; Talarmin, J. *J. Electroanal. Chem.* **2007**, *603*, 15−20.

(15) (a) Pombeiro, A. J. L.; Guedes da Silva, M. F. C.; Lemos, M. A. N. D. A. *Coord. Chem. Rev.* **2001**, *219*−*221*, 53−80. (b) Guedes da Silva, M. F. C.; Ferreira, C. M. P.; Fraústo da Silva, J. J. R.; Pombeiro, A. J. L. *J. Chem. Soc., Dalton Trans.* **1998**, 4139−4145. (c) Geiger, W. E.; Shaw, M. J.; Wünsch, M.; Barnes, C. E.; Foersterling, F. H. *J. Am. Chem. Soc.* **1997**, *119*, 2804−2811. (d) Mevs, J. M.; Geiger, W. E. *J. Am. Chem. Soc.* **1989**, *111*, 1922−1923. (e) Connelly, N. G.; Raven, S. J.; Carriedo, G. A.; Riera, V *J. Chem. Soc., Chem. Commun.* **1986**, 992−993. (f) El Kbir, L.; Patin, H.; Darchen, A. *Organometallics* **1984**, *3*, 1128−1129. (g) Rieke, R. D.; Kojima, H.; Saji, T.; Rechberger, P.; Öfele, K. *Organometallics* **1988**, *7*, 749−755 and references therein.

(16) Gao, W.; Ekström, J.; Liu, J.; Chen, C.; Eriksson, L.; Weng, L.; Åkermark, B.; Sun, L. *Inorg. Chem.* **2007**, *46*, 1981−1991.

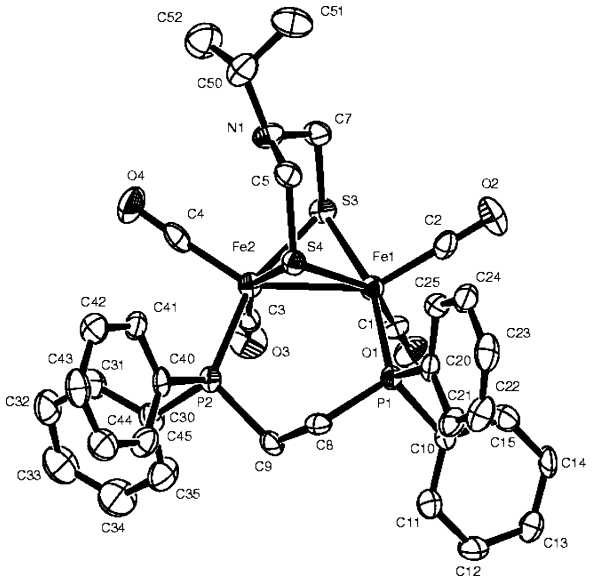

Figure 6. Structure of $[Fe_2(CO)_4(\mu\text{-}SCH_2N(^iPr)CH_2S)(\mu\text{-dppe})]$ (**2a**) with thermal ellipsoids at 30% probability (a molecule of CH_2Cl_2 is omitted).

Table 3. Selected Bond Lengths (Å) and Angles (deg) for **2a**

Fe1−Fe2	2.5446(11)		
Fe1−S3	2.2519(17)	Fe2−S3	2.2519(17)
Fe1−S4	2.2584(16)	Fe2−S4	2.2481(16)
Fe1−P1	2.2294(17)	Fe2−P2	2.2187(17)
C5−N1	1.436(7)	C7−N1	1.443(7)
C50−N1	1.495(7)	C5−S4	1.837(6)
C7−S3	1.836(6)		
Fe1−C1	1.752(7)	C1−O1	1.173(7)
Fe1−C2	1.775(7)	C2−O2	1.145(6)
Fe2−C3	1.769(7)	C3−O3	1.156(6)
Fe2−C4	1.777(7)	C4−O4	1.154(6)
Fe1−S3−Fe2	68.79(5)	Fe1−S4−Fe2	68.76(5)
C5−N1−C7	113.1(5)	C5−N1−C50	113.4(5)
C7−N1−C50	113.8(5)		

the $\{Fe(CO)_3\}$ and $\{Fe(CO)P_2\}$ moieties, respectively. For **2d**, two doublets (J = 21 and 8 Hz) are detected at 215.2 and 214.3 ppm. This pattern accords with the expected signals for two equivalent $\{(Fe(CO)_2P\}$ moieties with two equivalent CO in basal position and two other lying in the apical orientation. Single crystals of **2a** and **2d** have been obtained. Only the X-ray analysis of **2a** afforded reliable results, which demonstrates without any ambiguity that the dppe ligand is symmetrically bridged between the two iron atoms in a cis dibasal position [Fe−P, 2.2294(17) and 2.2187(17) Å] (Figure 6 and Table 3).

Reductive Electrochemistry of $[Fe_2(CO)_4(\mu\text{-}SCH_2XCH_2S)(\mu\text{-dppe})]$ (X = N^iPr), 2a; NCH_2CH_2OMe, 2b; CH_2, 2d) and a Proposed Mechanism for the ETC Isomerization. Previous studies of $[Fe_2(CO)_6(\mu\text{-dithiolate})]$ complexes (dithiolate = pdt or $S(C_6H_4)S$, bdt)[14] showed that dianionic species are involved in ETC substitutions of $P(OMe)_3$ for CO (two-electron-transfer catalysis[14a]). In order to assess whether this is also a possibility for the ETC rearrangement of **1**, it is necessary to investigate the electrochemical reduction of both **1** and **2**. Unfortunately, the very occurrence of the ETC-catalyzed process precludes a detailed analysis of the reduction mechanism of **1**, and of the reactivity of $\mathbf{1}^-$ toward CO.[17] However, this can be done for **2**.

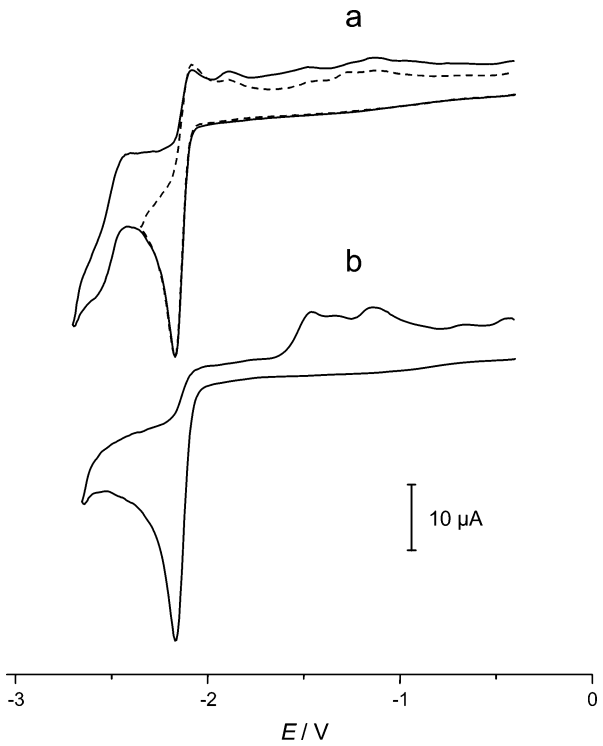

Figure 7. Cyclic voltammetry of $[Fe_2(CO)_4\{\mu\text{-}SCH_2N(^iPr)CH_2S\}(\mu\text{-dppe})]$ (**2a**) (1 mM) in MeCN−$[NBu_4][PF_6]$ (a) under Ar and (b) under CO; in (a) the dashed line shows the CV scan limited to the primary reduction of **2a** (v = 0.2 V s^{-1}, vitreous carbon electrode).

The CVs of the fully characterized **2a**,**b**,**d** in MeCN− or THF−$[NBu_4][PF_6]$ confirm that the major reduction peak observed in the CV of **1a**,**b**,**d** is due to the symmetrical isomer (compare Figures 3a and 7a) that undergo reduction and oxidation steps at potentials respectively more negative and more positive than those of the unsymmetrical isomers (Table 2). This indicates a larger HOMO−LUMO separation in the diphos-bridged vs -chelated isomers. The reduction of complexes **2a**−**b** is a partially reversible process followed by chemical reactions (EC mechanism)[13,18] whose products are detected by the presence of a quasi-reversible reduction around −2.4 (MeCN) or −2.6 V (THF), as well as by several oxidation peaks on the return scan (Figures 7a and S4, Supporting Information) that result from the fragmentation of the reduced species. In agreement with an EC mechanism, these processes are suppressed upon increasing the scan rate or lowering the temperature. Comparison of the current functions of **2a** and **2d** [i_p^{red}(**2*i***)/$v^{1/2}$] (***i*** = **a** or **d**) at different scan rates to the current function of the reversible, diffusion-controlled, one-electron oxidation of $[Fe_2(CO)_4(I_{Me}-CH_2-I_{Me})(\mu\text{-pdt})]$[8] ($I_{Me}$ = 1-methylimidazol-2-ylidene) under identical conditions (Figure 8) clearly shows that the reduction of the (μ-dppe) complexes is not a simple one-electron process.[19] Because of the similarity of the reductive behavior

(17) The reduction of complex **1** can be studied at low temperature, that is, under conditions that prevent the ETC process and restrict a possible reaction of $\mathbf{1}^-$ with CO.

(18) (a) Bard, A. J.; Faulkner, L. R. *Electrochemical Methods. Fundamentals and Applications*; Wiley: New York, 1980; Chapter 11, pp 429−485. (b) Brown, E. R.; Large, R. F. In *Techniques of Chemistry, Vol. I—Physical Methods of Chemistry*, Part IIA; Weissberger, A., Ed.; Wiley, 1971; Chapter 6, pp 423−530.

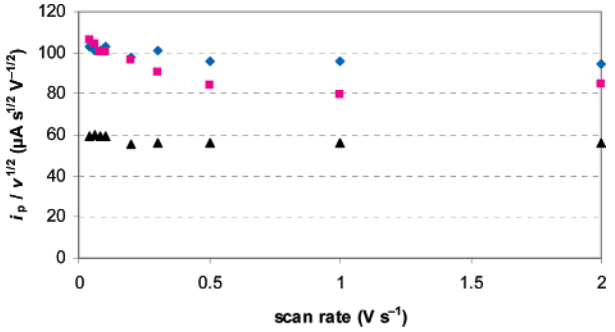

Figure 8. Scan rate dependence of the current function for the reduction of 1 mM solutions of (◆) $[Fe_2(CO)_4\{\mu\text{-}SCH_2N(^iPr)CH_2S\}(\mu\text{-dppe})]$ (**2a**), (■) $[Fe_2(CO)_4(\mu\text{-pdt})(\mu\text{-dppe})]$ (**2d**), and for the oxidation of a 1 mM solution of $[Fe_2(CO)_4(\mu\text{-pdt})(I_{Me}-CH_2-I_{Me})]$ (▲) in MeCN−$[NBu_4][PF_6]$.

of both azadithiolate-bridged derivatives, this should also be true for **2b**. However, differences emerge between the azadithiolate complexes **2a**−**b** and the propanedithiolate analogue **2d**. As shown in Figure 8, the current function deviates noticeably from linearity at slow scan rates ($\upsilon < 1$ V s^{-1}) for **2d** while it is essentially independent of υ over the range 0.04 V $s^{-1} \leq \upsilon \leq 2$ V s^{-1} for **2a**. This suggests the possible contribution of an ECE process for **2c** that would be absent for **2a** (EC process, see above).[18] Furthermore, the scan rate dependence of $[(i_p^a/i_p^c)^{red}(\mathbf{2}\boldsymbol{i})]$[13] (***i*** = **a**, **b**, or **d**) indicates that the reduction of the azadithiolate complexes **2a**−**b** is chemically more reversible than that of the pdt analogue when identical conditions of scan rate and concentration apply. These results confirm that the nature of the S-to-S link introduces subtle differences in the electrochemical behavior of closely related complexes, as we already noted for the hexacarbonyl precursors of **2a**,**b**,**d**.[28] From the above results it can be concluded that the reduction of the (μ-dppe) complexes comprises two one-electron steps

Scheme 5

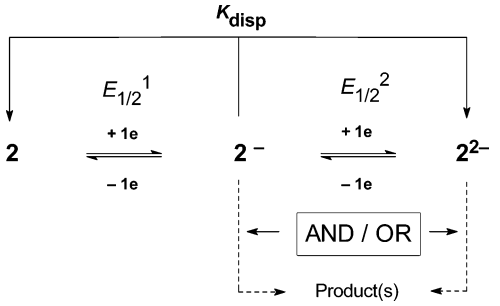

Scheme 6

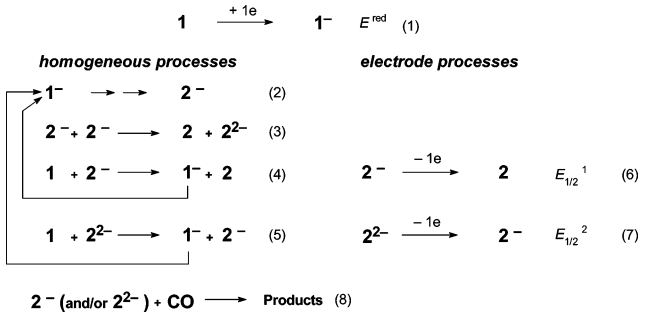

($E_{1/2}^1$, $E_{1/2}^2$) that cannot be separated by CV at fast scan rates, in contrast to their hexacarbonyl parents.[28] Digital simulations[19b] of cyclic voltammograms indicate that the experimental data are consistent with an EE reduction where the individual redox steps have similar rate constants k_s and potentials such that $E_{1/2}^2 - E_{1/2}^1 \geq 0$. As a consequence, the reduction mechanism of **2a**−**d** (Scheme 5) includes the disproportionation of the anion. The follow-up reactions, evidenced by the presence of product peaks in the CVs (see above), are assumed to consist initially in Fe−S bond(s) cleavage, but they were not investigated in detail. Further studies are clearly needed to identify the factors that turn the electrochemical reduction of closely related $[Fe_2(CO)_4(L)_2(\mu\text{-dithiolate})]$ complexes (L = phosphine, phosphite or $(L)_2$ = diphosphine) into either a two-electron[15a,29,30] or a one-electron[31,32] process.

When CO is present, the reduction of **2** is chemically much less reversible than under Ar (for identical υ), and the quasi-reversible system around −2.4 (MeCN) or −2.6 V (THF) is absent (Figures 7b and S4).[33] The reaction of $\mathbf{2}^-$ (and $\mathbf{2}^{2-}$) with CO provides a rationale for the inhibiting effect of CO on the catalytic isomerization of **1**, although it does preclude the possibility that $\mathbf{1}^-$ also reacts with CO.[17]

(19) (a) This is based on the reasonable assumption that the diffusion coefficients of **2** and of $[Fe_2(CO)_4(\mu\text{-pdt})(I_{Me}-CH_2-I_{Me})]$ are similar. The reduction current of **2a** was also compared to the first oxidation peak current of $[Fe_2Cp_2(CO)_2(\mu\text{-SMe})_2]$ ($[i_p^{ox}(1e)]$, reversible one-electron oxidation[20]), and to the reduction peak current of $[Fe_2(CO)_6(\mu\text{-bdt})]$ ($[i_p^{red}(2e)]$, reversible two-electron reduction with $E^\circ_2 - E^\circ_1 > 0$ [21]) at the same concentrations as **2a** in MeCN−$[NBu_4][PF_6]$. This confirmed that two electrons are involved in the reduction of **2a**, with $[i_p^{red}(\mathbf{2a})]/[i_p^{ox}(1e)] \cong 2.5$ and $[i_p^{red}(\mathbf{2a})]/[i_p^{red}(2e)] \cong 0.7$. Note that the current function of a 2e⁻-transfer step is 2.83 ($2^{3/2}$) times that of a 1e⁻-transfer when the second electron transfer is thermodynamically more favourable than the first one ($E^\circ_2 - E^\circ_1 > 0$), and 2.41 times that of a 1e⁻-transfer when both electrons are transferred at the same potential ($E^\circ_2 = E^\circ_1$), in case of fast heterogeneous charge-transfer reactions.[18,22−25] (b) Simulations of CV curves using DigiElch (version 2 or 3) [26] confirmed that the magnitudes of the peak current and of the peak-to-peak separation of a two-electron transfer process are affected by the rate constants of the heterogeneous electron-transfer (k_s) when $\Delta E^\circ = E^\circ_2 - E^\circ_1 >$ ca 0.1 V, see Supporting Information. (c) The above method was preferred to coulometry to derive the number of electrons involved in the reduction of **2** on short time scales because follow-up reactions (that are detected by CV at slow scan rate) may be prominent on the longer time scale of bulk electrolyses; the following chemistry is thus susceptible to affect the coulometrically measured *n* value.[27] Exhaustive electrolyses of **2a** and **2d** require that a charge > 2 F mol^{-1} starting material be passed and produce uncharacterized products.

(20) (a) Gennett, T.; Geiger, W. E.; Willett, B.; Anson, F. C. *J. Electroanal. Chem.* **1987**, *222*, 151−160. (b) Madec, P.; Muir, K. W.; Pétillon, F.Y.; Rumin, R.; Scaon, Y.; Schollhammer, P.; Talarmin, J. *J. Chem. Soc., Dalton Trans.* **1999**, 2371−2383.

(21) Capon, J.-F.; Gloaguen, F.; Schollhammer, P.; Talarmin, J. *J. Electroanal. Chem.* **2004**, *566*, 241−247.

(22) Polcyn, D. S.; Shain, I. *Anal. Chem.* **1966**, *38*, 366−375.

(23) Savéant, J.-M. *Elements of Molecular and Biomolecular Electrochemistry—An Electrochemical Approach to Electron Transfer Chemistry*; Wiley: New York, 2006; Chapter 1, pp 62−77.

(24) Heinze, J. *Angew. Chem., Int. Ed. Engl.* **1984**, *23*, 831−847.

(25) Ryan, M. D. *J. Electrochem. Soc.* **1978**, *125*, 547−555.

(26) For detailed information concerning DigiElch, see www.elchsoft.com and the following papers: (a) Rudolph, M. *J. Electroanal. Chem.* **2003**, *543*, 23−29. (b) Rudolph, M. *J. Electroanal. Chem.* **2004**, *571*, 289−307. (c) Rudolph, M. *J. Comput. Chem.* **2005**, *26*, 619−632. (d) Rudolph, M. *J. Comput. Chem.* **2005**, *26*, 633−641. (e) M. Rudolph, *J. Comput. Chem.* **2005**, *26*, 1193−1204.

(27) Pierce, D. T.; Geiger, W. E. *J. Am. Chem. Soc.* **1992**, *114*, 6063−6073.

(28) Capon, J.-F.; Ezzaher, S.; Gloaguen, F.; Pétillon, F. Y.; Schollhammer, P.; Talarmin, J.; Davin, T. J.; McGrady, J. E.; Muir, K. W. *New J. Chem.* **2007**, DOI 10.1039/b709273c.

Table 4. Crystallographic Data for Complexes **1a**−**c** and **2a**

	1a	**1b**	**1c**	**2a**
empirical formula	$C_{35}H_{35}Fe_2NO_4P_2S_2$	$C_{35}H_{35}Fe_2NO_5P_2S_2$	$C_{39}H_{35}Fe_2NO_4P_2S_2$	$C_{36}H_{37}Cl_2Fe_2NO_4P_2S_2$
fw	771.40	787.40	819.44	856.33
T/K	170(2)	295(2)	170(2)	170(2)
cryst syst	monoclinic	monoclinic	monoclinic	monoclinic
space group	$P2_{1/n}$	$C2/c$	$P2_1/c$	$P2_1/c$
a(Å)	10.9362 (8)	34.495 (5)	11.0438(6)	11.1813(7)
b(Å)	10.7765(8)	11.8409(9)	22.4200(14)	22.9345(15)
c(Å)	30.1258(16)	20.873(3)	14.8519(9)	15.1949(10)
α(°)	90	90	90	90
β(°)	93.908(5)	123.853(19)	96.859(6)	98.029(6)
γ(°)	90	90	90	90
V(Å^3)	3542.2(4)	7080.3(15)	3651.0(4)	3858
Z	4	8	4	4
ρ_{calcd} (mg mm^{-3})	1.446	1.477	1.491	1.474
μ (mm^{-1})	1.066	1.070	1.039	1.120
crystal size (mm^3)	0.24 × 0.18 × 0.05	0.13 × 0.09 × 0.08	0.16 × 0.09 × 0.04	0.22 × 0.07 × 0.05
range of θ (°)	2.66−28.85	3.29−23.26	2.84−23.26	3.24−23.26
reflns measured	21 064	19 820	14 883	9335
R_{int}	0.0427	0.0683	0.0782	0.0519
unique data/params	7100/417	4767/425	4968/451	5389/444
R1 [$I > 2\sigma(I)$]	0.0489	0.0546	0.0538	0.0541
R1 (all data)	0.0921	0.1036	0.1096	0.0954
wR2 (all data)	0.1225	0.1047	0.0799	0.1150
GOF on F^2	1.081	1.019	0.958	0.965
$\Delta\rho_{max,}\Delta\rho_{min}$/e Å^{-3}	0.761, −0.616	0.271, −0.446	0.382,−0.360	0.456,−0.455

Scheme 7. X = N(R) (**1a/2a** and **1b/2b**) or CH_2 (**1d/2d**); the Species in Braces Are Postulated

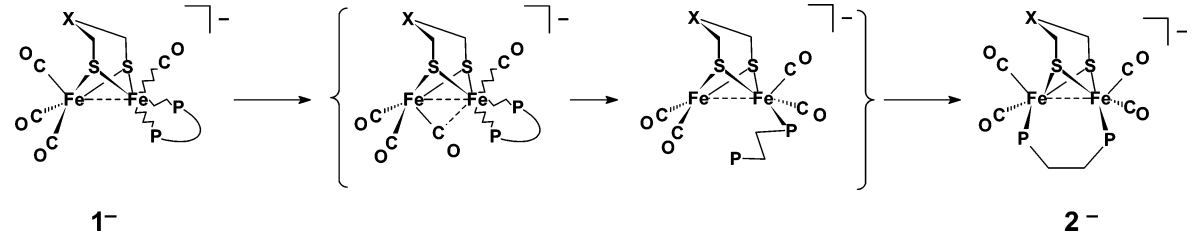

From these results, the reactions in Scheme 6 are proposed to account for the ETC rearrangement of **1** under an inert atmosphere (eqs 1−7) and for its inhibition by CO (eq 8). As noted above, the reduction of **1** could not be investigated electrochemically under conditions that allow the ETC-catalyzed isomerization to occur,[17] so whether or not $\mathbf{1}^{2-}$ is generated and contributes to the catalytic isomerization cannot be established.[34] The contribution of $\mathbf{2}^{2-}$ is shown in Scheme 6 (eqs 5 and 7) due to the potential disproportionation of $\mathbf{2}^{-}$ (eq 3, Scheme 6).[28]

The mechanism of the isomerization step (eq 2, Scheme 6) that initiates the catalytic process is of particular interest in connection with the design and reactivity of unsymmetrical models of the [FeFe]-H_2ase active site. DFT calculations have shown that the presence of donor ligands in unsymmetrically substituted [$Fe_2(CO)_4L_2$(μ-dithiolate)] complexes favors the "*rotated*" geometry where a CO ligand lies beneath the Fe−Fe bond.[4] DFT analysis of the substitution of PMe_3 for CO in complexes closely related to **1**, namely [$Fe_2(CO)_4$(dppv)(μ-dithiolate)] (dppv = *cis*-$Ph_2PCH{=}CHPPh_2$), pointed out that the electron-richness of the Fe(CO)(dppv) fragment assists the rotation of the $Fe(CO)_3$ group and the formation of a bridging CO in the transition state.[5] It is conceivable that the rotation of the $Fe(CO)_3$ fragment could also be facilitated by the weakening of the Fe−Fe bond in the one-electron-reduced form of the complex ($\mathbf{1}^{-}$), where the CO in a semi-bridging position would contribute to relief of the

(29) Mathieu, R.; Poilblanc, R.; Lemoine, P.; Gross, M. *J. Organomet. Chem.* **1979**, *165*, 243−252.
(30) Gloaguen, F.; Morvan, D.; Capon, J.-F.; Schollhammer, P.; Talarmin, J. *Eur. J. Inorg. Chem.* **2007**, submitted for publication.
(31) (a) Gao, W.; Ekström, J.; Liu, J.; Eriksson, L.; Weng, L.; Åkermark, B.; Sun, L. *Inorg. Chem.* **2007**, *46*, 1981−1991. (b) Dong, W.; Wang, M.; Liu, T.; Liu, X.; Jin, K.; Sun, L. *J. Inorg. Biochem.* **2007**, *101*, 506−513. (c) Na, Y.; Wang, M.; Jin, K.; Zhang, R.; Sun, L. *J. Organomet. Chem.* **2006**, *691*, 5045−5051. (d) Li, P.; Wang, M.; He, C.; Li, G.; Liu, X.; Chen, C.; Åkermark, B.; Sun, L. *Eur. J. Inorg. Chem.* **2005**, 2506−2513.
(32) (a) Mejia-Rodriguez, R.; Chong, D.; Reibenspies, J. H.; Soriaga, M. P.; Darensbourg, M. Y. *J. Am. Chem. Soc.* **2004**, *126*, 12004−12014. (b) Chong, D.; Georgakaki, I. P.; Mejia-Rodriguez, R.; Sanabria-Chinchilla, J.; Soriaga, M. P.; Darensbourg, M. Y. *Dalton Trans.* **2003**, 4158−4163.
(33) (a) The overall two-electron reduction of **2** is likely to involve structural change, such as Fe−S bond cleavage, at some stage of the process.[33b] The characteristics of the redox process suggest that the structure change is reversible under Ar while a reduced species is irreversibly trapped by CO, making the overall reduction irreversible. This is quite similar to the CO effect on the electrochemical reduction of [Fe_2-$(CO)_5$(μ-pdt)(I_{Me})].[28] (b) For a discussion of structural consequences of electron-transfer steps, see: (i) Geiger, W. E. *Prog. Inorg. Chem.* **1985**, *33*, 275−352. (ii) Evans, D. H.; O'Connell, K. M. In *Electroanalytical Chemistry*; Bard, A. J., Ed.; Marcel Dekker: New York, 1986; Vol. 14, pp 113−207. (iii) Pétillon, F. Y.; Schollhammer, P.; Talarmin, J. In *Encyclopedia of Electrochemistry*; Bard, A. J., Stratman, M., Eds.; Wiley: New York, 2006; Vol. 7b, pp 565−590. (iv) Uhrhammer, D.; Schultz, F. A. *J. Phys. Chem. A* **2002**, *106*, 11630−11636, and references therein.
(34) If $\mathbf{1}^{2-}$ is generated upon reduction of **1**, the isomerization step may involve anionic ($\mathbf{1}^{-} \rightarrow \mathbf{2}^{-}$) and/or dianionic ($\mathbf{1}^{2-} \rightarrow \mathbf{2}^{2-}$) species.

electronic strain on the disubstituted iron center.[35] Whether the full migration of this CO from one iron center to the other causes, results from, or is concerted with, the decoordination of one end of the diphosphine chelate (Scheme 7) is not known. In the proposed mechanism, the rearrangement of the anionic complex is completed by the binding of the dangling phosphorus atom to the coordinatively unsaturated iron center. This latter step might understandably be hindered under a CO atmosphere due to competitive CO binding to the exposed coordination site, which is a possible deactivation pathway of the ETC isomerization in addition to the reaction of $\mathbf{2}^-$ (and/or $\mathbf{2}^{2-}$) with CO.[33] A rotated geometry was also recently proposed to result from the electrochemical reduction of a phosphine singly substituted diiron dithiolate complex.[36] However, DFT calculations on this model complex suggested that one Fe−S bond was cleaved in the μ-CO species.[37] In the case of our complexes, the contribution of an intermediate with a terminally bound S ligand to the $\mathbf{1}^- \rightarrow \mathbf{2}^-$ isomerization process is also a possibility.

Electronic factors that were reported to favor the rotated geometry in diiron dithiolate complexes may thus be important to the occurrence of the ETC isomerization. However, they are not decisive since such a catalytic rearrangement was not detected for $[Fe_2(CO)_4(I_{Me}-CH_2-I_{Me})(\mu\text{-pdt})]$, which is another type of unsymmetrically disubstituted model complex that reduces at a potential more negative than **1**.[8] Besides the electronic properties of the chelating ligand, its nature is clearly a central aspect of the resistance of the unsymmetrical structure to isomerization upon reduction, and further studies with other diphosphine ligands are underway to explore this issue.

Conclusion

In this paper we report the first example of an ETC isomerization of four $[Fe_2(CO)_4(\kappa^2\text{-dppe})(\mu\text{-dithiolate})]$ complexes to the symmetrical (μ-dppe) isomer. Although the electron-releasing properties of the chelating ligand are probably important as to the occurrence of the catalytic isomerization, electrochemical studies of unsymmetrical complexes are still too rare to precisely identify the factors that control the fate of their reduced forms. Further studies of unsymmetrically disubstituted diphosphine complexes are now underway in our laboratory since this kind of compound, with well-differentiated iron centers, bear more resemblance with the [2Fe] subsite of the H-cluster than their symmetrical isomers, and thus are more attractive models of the [FeFe]-hydrogenases.

Experimental Section

Methods and Materials. All the experiments were carried out under an inert atmosphere, using Schlenk techniques for the syntheses. Tetrahydrofuran (THF) was purified as described previously.[38] Acetonitrile (Merck, HPLC grade) was used as received. $[Fe_2(CO)_4(\kappa^2\text{-dppe})(\mu\text{-S(CH}_2)_3\text{S})]$[9] (**1d**) and $[Fe_2(CO)_6\{\mu\text{-SCH}_2\text{N(R)CH}_2\text{S}\}]$ (R = ^{i}Pr,[28] CH_2CH_2OMe,[28] $CH_2C_6H_5$[39]) were prepared according to the reported procedure. The preparation and the purification of the supporting electrolyte $[NBu_4][PF_6]$ were described previously.[38] The electrochemical equipment consisted either in a GCU potentiostat (Tacussel/Radiometer) driven by a PAR 175 Universal Programmer (CV traces were recorded with a SEFRAM TGM 164 X-Y recorder) or a μ-AUTOLAB (Type III) driven by a GPES software. Controlled-potential electrolyses were performed using a GCU potentiostat and an IG5-N (Tacussel/Radiometer) integrator. The cell and electrodes were as described previously.[38] All the potentials (text, tables, figures) are quoted against the ferrocene−ferrocenium couple; ferrocene was added as an internal standard at the end of the experiments. The NMR spectra (^{1}H, ^{13}C, ^{31}P) were recorded at room temperature in CD_2Cl_2, $CDCl_3$, or C_6D_6 solutions with a Bruker AMX 400 or AC300 spectrometer and were referenced to $SiMe_4$(^{1}H) and H_3PO_4 (^{31}P). ^{1}H−^{13}C experiments were carried out on a Bruker DRX 500 spectrometer. The infrared spectra were recorded on a Nicolet Nexus Fourier transform spectrometer. Chemical analyses were made by the Service de Microanalyses I.C.S.N., Gif sur Yvette, France or the Centre de Microanalyses du CNRS, Vernaison (France). Crystal data (Table 4) for compounds **1a**−**c** and **2a** were collected on a Oxford Diffraction X-Calibur-2 CCD diffractometer, equipped with a jet cooler device and graphite-monochromated Mo Kα radiation (λ = 0.71073 Å). The structures were solved and refined by standard procedures.[40]

Synthesis of $[Fe_2(CO)_4(\kappa^2\text{-dppe})\{\mu\text{-SCH}_2\text{N(R)CH}_2\text{S}\}]$ (R = ^{i}Pr, 1a; CH_2CH_2OMe, 1b; $CH_2C_6H_5$, 1c). In a typical procedure, a solution of the azadithiolate hexacarbonyl derivative $[Fe_2(CO)_6\{\mu\text{-SCH}_2\text{N(R)CH}_2\text{S}\}]$ (0.2 g, 0.47 mmol, R = ^{i}Pr; 0.3 g, 0.675 mmol, R = CH_2CH_2OMe; 0.24 g, 0.507 mmol, R = $CH_2C_6H_5$) and 2 equiv of dppe (0.37 g, 0.932 mmol; 0.54 g, 1.35 mmol; 0.40 g, 1.014 mmol, respectively) in THF (100 mL) was heated in the presence of 2 equiv of $Me_3NO,2H_2O$ (0.16 g, 0.978 mmol; 0.23 g, 1.42 mmol; 0.18 g, 1.065 mmol, respectively) at 70 °C for 4 h. The initially orange solution became brownish. After evaporation of the solvent, the residue was chromatographed on a silica gel column. Elution with hexane−dichloromethane mixtures afforded a brownish solution of **1** which was evaporated under vacuum. Compounds **1a**−**c** were washed with pentane and obtained as brownish air-stable powders (**1a**, 0.16 g, 39% yield; **1b**, 0.22 g, 41% yield; **1c**, 0.20 g, 47% yield). Crystals of **1a**−**c**, suitable for X-ray analysis, were formed by crystallization at room temperature from CH_2Cl_2/Et_2O solutions. **1a**. IR (CH_2Cl_2, cm^{-1}): ν(CO) 2019(s), 1953(s), 1941(s), 1903(w). ^{1}H NMR (CD_2Cl_2, 25 °C): major isomer, 7.95−7.20 (m, 20H, C_6H_5), 2.94 (m, 2H, PCH_2CH_2P), 2.74 (d, 2H, J = 10.8 Hz, $(\mu\text{-SCH}_2)_2$N), 2.70 (m, 2H, PCH_2CH_2P), 2.29 (spt, 1H, J = 6.6 Hz, ^{i}Pr), 1.75 (d, 2H, J = 10.8 Hz, $(\mu\text{-SCH}_2)_2$N), 0.47 ppm (d, 6H, J = 6.6 Hz, ^{i}Pr); minor isomer, 7.95−7.20 (m, 20H, C_6H_5), 3.35 (d, J = 12.5 Hz, $(\mu\text{-SCH}_2)_2$N), 3.15 (d, 2H, J =

(35) For discussions on the contribution of semi-bridging CO in redressing the charge imbalance between two metal centres, see: (a) Cotton, F. A.; Troup, J. M. *J. Am. Chem. Soc.* **1974**, *96*, 1233−1234. (b) Cotton, F. A. *Prog. Inorg. Chem.* **1976**, *21*, 1. (c) Bino, A.; Cotton, F. A.; Lahuerta, P.; Puebla, P.; Uson, R. *Inorg. Chem.* **1980**, *19*, 2357−2359. (d) Crabtree, R. H.; Lavin, M. *Inorg. Chem.* **1986**, *25*, 805−812. (e) Baxter, R. J.; Knox, G. R.; Pauson, P. L.; Spicer, M. D. *Organometallics* **1999**, *18*, 215−218, and references therein.

(36) Hou, J.; Peng, X.; Zhou, Z.; Sun, S.; Zhao, X.; Gao, S. *J. Organomet. Chem.* **2006**, *691*, 4633−4640.

(37) Greco, C.; Bruschi, M.; Fantucci, P.; de Gioia, L. *Eur. J. Inorg. Chem.* **2007**, 1835−1843.

(38) Cabon, J.-Y.; Le Roy, C.; Muir, K. W.; Pétillon, F. Y.; Quentel, F.; Schollhammer, P.; Talarmin, J. *Chem.−Eur. J.* **2000**, *6*, 3033−3042.

(39) Lawrence, J. D.; Li, H.; Rauchfuss, T. B. *Chem. Commun.* **2001**, 1482−1483.

(40) Programs used: (a) Sheldrick, G. M. *SHELX97*; University of Göttingen: Göttingen, Germany, 1998. (b) WinGX - A Windows Program for Crystal Structure Analysis (Farrugia, L. J. *J. Appl. Crystallogr.* **1999**, *32*, 837).

12.5 Hz, (μ-SCH_2)$_2$N), 2.94 (m, 2H, PCH_2CH_2P), 2.60 (m, 2H, PCH_2CH_2P), 2.76 (spt, 1H, J = 6.6 Hz, ^{i}Pr), 0.94 ppm (d, 6H, J = 6.6 Hz, ^{i}Pr). $^{31}P\{^1H\}$ NMR (CD_2Cl_2, 25 °C): 92.1 (s) (major isomer, 80%), 78.1 ppm (s) (minor isomer, 20%). Anal. Calcd (%) for $C_{35}H_{35}Fe_2NO_4P_2S_2$: C, 54.49; H, 4.57; N, 1.82; P, 8.03. Found: C, 53.65; H, 4.61; N, 1.74; P, 7.82. **1b**. IR (CH_2Cl_2, cm^{-1}): ν(CO) 2019(s), 1949(s), 1941(sh), 1905(w). ^1H NMR (CD_2Cl_2, 25 °C): major isomer, 7.95−7.20 (m, 20H, C_6H_5), 3.03 (s, 3H, OCH_3), 2.81 (t, J = 5.5 Hz, 2H, NCH_2CH_2O), 2.78 (m, 2H, PCH_2CH_2P), 2.75 (d, 2H, J = 11.3 Hz, (μ-SCH_2)$_2$N), 2.67 (m, 2H, PCH_2CH_2P), 2.30 (d, J = 11.3 Hz, 2H, (μ-SCH_2)$_2$N), 2.11 ppm (t, J = 5.5 Hz, 2H, NCH_2CH_2O); $^{31}P\{^1H\}$ NMR (CD_2Cl_2, 25 °C): 91.1 (s) (major isomer, 78%), 75.2 ppm (s) (minor isomer, 22%). Anal. Calcd (%) for $C_{35}H_{35}Fe_2NO_5P_2S_2$: C, 53.39; H, 4.48; N, 1.78; P, 7.86. Found: C, 53.96; H, 4.32; N, 1.58; P, 8.34. **1c**. IR (CH_2Cl_2, cm^{-1}): ν(CO) 2020(s), 1951(s), 1941(s), 1905(w). ^1H NMR (CD_2Cl_2, 25 °C): major isomer, 7.85−7.70 (m, 25H, C_6H_5), 2.80 (m, 2H, PCH_2CH_2P), 2.72 (m, 2H, PCH_2CH_2P), 2.68 (d, 2H, J = 11.1 Hz, (μ-SCH_2)$_2$N), 3.01 (s, 2H, $NCH_2C_6H_5$), 2.13 ppm (d, J = 11.1 Hz, (μ-SCH_2)$_2$N). $^{31}P\{^1H\}$ NMR (CD_2Cl_2, 25 °C): 92.0 (s) (major isomer, 80%), 77.8 ppm (s) (minor isomer, 20%). Anal. Calcd (%) for $C_{39}H_{35}Fe_2NO_4P_2S_2{\cdot}H_2O$: C, 55.93; H, 4.45; N, 1.67; P, 7.52. Found: C, 55.62; H, 4.29; N, 1.53; P, 7.40.

Electrosynthesis of [$Fe_2(CO)_4${μ-$SCH_2N(R)CH_2S$}(μ-dppe)] (R = ^{i}Pr, 2a; CH_2CH_2OMe, 2b; CH2Ph, 2c) and of [$Fe_2(CO)_4$(μ-pdt)(μ-dppe)] (2d). In a typical experiment, 0.1 g (1.4 10^{-4} mol) of complex **1d** was dissolved in 25 mL THF−[NBu_4][PF_6] in the electrochemical cell. The potential of the graphite cathode was set at −2.1 V and the electrolysis was started. The cell current decayed to the background level after the passage of 1.6 C (0.12 F mol^{-1} **1d**). The electrolysis was stopped, and CV of the electrolyzed solution showed that **2d** was formed almost quantitatively (ca 90%). The catholyte was cannulated in a Schlenk flask under dinitrogen. The solution was then taken down to dryness and the solid residue extracted by 3 × 50 mL of diethyl ether in order to separate the electrolysis product from the supporting electrolyte. After evaporation of the solvent, the solid was dried under vacuum. This afforded 0.073 g (73%) of **2d**. A similar procedure was followed to obtain **2a** (0.072 g, 36% yield), **2b** (0.135 g, 96% yield), and **2c** (0.54 g, 54% yield) from **1a** (0.2 g), **1b** (0.14 g), and **1c** (0.1 g), respectively. Crystals of **2a**, suitable for X-ray analysis, were formed by crystallization at room temperature from CH_2Cl_2/Et_2O solutions. **2a**. IR (CH_2Cl_2, cm^{-1}): ν(CO) 1989(s), 1954(s), 1921(s), 1902(w). ^1H NMR (CD_2Cl_2, 25 °C): 7.95−7.20 (m, 20H, C_6H_5), 3.56 (m, 2H, PCH_2CH_2P), 3.34 (m, 2H, PCH_2CH_2P), 3.08 (spt, 1H, J = 6.5 Hz, ^{i}Pr), 2.33 (m, 4H, (μ-SCH_2)$_2$N), 1.07 ppm (d, 6H, J = 6.5 Hz, ^{i}Pr). $^{31}P\{^1H\}$ NMR (CD_2Cl_2, 25 °C): 61.3 ppm (s). Anal. Calcd (%) for $C_{35}H_{35}Fe_2NO_4P_2S_2$: C, 54.49; H, 4.57; N, 1.82. Found: C, 54.33; H, 4.97; N, 1.51. **2b**. IR (CH_2Cl_2, cm^{-1}): ν(CO) 1989(s), 1952(s), 1920(s), 1901(w). ^1H NMR (CD_2Cl_2, 25 °C): 7.80−7.45 (m, 20H, C_6H_5), 4.03 (m, 2H, PCH_2CH_2P), 3.75 (m, 2H, PCH_2CH_2P), 3.38 (t, J = 5.5 Hz, 2H, NCH_2CH_2O), 3.32 (s, 3H, OCH_3), 3.26 (t, J = 5.5 Hz, 2H, NCH_2CH_2O), 2.33 ppm (m, 4H, (μ-SCH_2)$_2$N). $^{31}P\{^1H\}$ NMR (CD_2Cl_2, 25 °C): 60.8 ppm (s). Anal. Calcd (%) for $C_{35}H_{35}Fe_2NO_5P_2S_2$: C, 53.39; H, 4.48; N, 1.78. Found: C, 53.85; H, 5.24; N, 1.23. **2c**. IR (CH_2Cl_2, cm^{-1}): ν(CO) 1990(s), 1955(s), 1922(s), 1902(w). ^1H NMR ($CDCl_3$, 25 °C): 7.74−7.26 (m, 25H, C_6H_5), 4.04 (s, 2H, $NCH_2C_6H_5$), 3.60 (m, 4H, PCH_2CH_2P), 2.30 ppm (m, 4H, (μ-SCH_2)$_2$N). $^{31}P\{^1H\}$ NMR ($CDCl_3$, 25 °C): 61.2 (s) ppm. **2d**. IR (CH_2Cl_2, cm^{-1}): ν(CO) 1989(s), 1953(s), 1920(s), 1901(w). ^1H NMR ($CDCl_3$, 25 °C): 7.74−7.26 (m, 20H, C_6H_5), 2.35 (m, 2H, PCH_2CH_2P), 2.11 (m, 2H, PCH_2CH_2P), 1.56 (m, 2H, μ-pdt), 1.39 (m, 2H, μ-pdt), 1.08 ppm (m,2H, μ-pdt). $^{31}P\{^1H\}$ NMR ($CDCl_3$, 25 °C): 60.3 ppm (s). Anal. Calcd (%) for $C_{33}H_{30}Fe_2O_4P_2S_2$: C, 54.42; H, 4.15; P, 8.52. Found: C, 54.64; H, 4.33; P, 7.67.

Acknowledgment. This work was supported by CNRS (Programme "Energie", PRI-4.1) and ANR (Programme "PhotoBioH2"). The Ministère de l'Education Nationale, de l'Enseignement Supérieur et de la Recherche is acknowledged for providing a studentship to S.E., and the Université de Bretagne Occidentale is acknowledged for financial support.

Supporting Information Available: Crystallographic information files (CIF) for **1a**−**c** and **2a**, and Figure S1 (CV of **1d** in MeCN−[NBu_4][PF_6]), Figure S2 (CV of **1b** in THF−[NBu_4][PF_6] under Ar and under CO), Figure S3 (CV of **1b** before and after controlled-potential electrolysis in MeCN−[NBu_4][PF_6]), Figure S4 (CV of **2d** in THF−[NBu_4][PF_6] under Ar and under CO) and digital simulations of 2e$^-$-transfer processes as pdf files. This material is available free of charge via the Internet at http://pubs.acs.org.

IC701327W